Journal of Catalysis 286 (2012) 124–136

Contents lists available at SciVerse ScienceDirect

Journal of Catalysis

journal homepage: www.elsevier.com/locate/jcat

Synthesis and hydrodesulfurization properties of NiW catalyst supported on high-aluminum-content, highly ordered, and hydrothermally stable Al-SBA-15

Yang Li [a,b], Dahai Pan [a], Chengzhong Yu [c,*], Yu Fan [a], Xiaojun Bao [a,b,*]

[a] State Key Laboratory of Heavy Oil Processing, China University of Petroleum, Changping, Beijing 102249, People's Republic of China
[b] The Key Laboratory of Catalysis, China National Petroleum Corporation, China University of Petroleum, Changping, Beijing 102249, People's Republic of China
[c] Department of Chemistry and Shanghai Key Laboratory of Molecular Catalysis and Innovative Materials, Fudan University, Shanghai 200433, People's Republic of China

ARTICLE INFO

Article history:
Received 16 September 2011
Revised 21 October 2011
Accepted 22 October 2011
Available online 7 December 2011

Keywords:
Al-SBA-15
pH adjustment
Hydrodesulfurization catalyst

ABSTRACT

Highly ordered mesoporous Al-SBA-15 with high aluminum content and high hydrothermal stability has been synthesized by a new pH-adjusting and high-temperature hydrothermal treatment approach. Thus-prepared samples were characterized by X-ray fluorescence spectroscopy, X-ray powder diffraction, ^{27}Al nuclear magnetic resonance spectroscopy, N_2 adsorption–desorption, temperature-programmed desorption of ammonia, Fourier transformed infrared spectroscopy with pyridine adsorption, temperature-programmed reduction with hydrogen, and high-resolution transmission electron microscopy. The results showed that Al-SBA-15 had high aluminum loading (with its molar Si/Al ratio of 5.1, similar to that of the initial gel mixture) and homogenously distributed Al species in the walls. Moreover, the product showed extremely high hydrothermal stability (with only a 15.2% decrease in surface area after steaming at 800 °C for 5 h) and moderate acidity. An Al-SBA-15-supported NiW hydrodesulfurization catalyst was prepared and evaluated using dibenzothiophene hydrodesulfurization. Compared with γ-Al_2O_3- and SBA-15-supported catalysts, the Al-SBA-15-supported NiW catalyst showed outstanding hydrodesulfurization activity.

1. Introduction

SBA-15 [1,2], a new type of ordered hexagonal-array mesoporous silica with two-dimensional *p6mm* hexagonal structure, one-dimensional channels, thicker walls, and much higher hydrothermal stability than M41S [3,4], has received much attention because of its favorable catalytic activities for reactions involving the conversion of bulkier molecules such as those of heavy crude oils and heavier petroleum fractions [5]. However, compared with conventional microporous zeolites, SBA-15 has much weaker acidity and lower hydrothermal stability because of its neutral Si frameworks. These two shortages severely limit its industrial applications, especially those dealing with high-temperature operations with steam, as encountered in petroleum fluid catalytic cracking (FCC), which needs acidic active sites strong enough to crack bulkier petroleum molecules to smaller ones in gasoline- and diesel-fraction ranges and in the hydrotreatment of petroleum refining products, which requires the involvement of acidic supports to favor hydrogenolysis/ring-opening and hydrogenation reactions [6]. Therefore, how to substantially improve the hydrothermal stability and acidity of SBA-15 has been the common focus of materials and catalysis sciences. To date, various metal-ion-substituted SBA-15 mesoporous materials have been prepared [7–9], in which partial replacement of Si^{4+} ions by Al^{3+} ions is a prior choice. This is because the ordered mesostructure and moderate acidity of Al-SBA-15 materials are desirable for reactions such as hydrodesulfurization (HDS) of dibenzothiophene (DBT) and alkyl-substituted DBTs that have relatively large kinetic diameters and steric hindrance and thus require catalysts with high accessibility and suitable Brønsted (B)/Lewis (L) acidities [10–12].

Incorporation of heteroatoms into pure silica SBA-15 can be achieved during the synthesis of the material or by various postsynthesis methods (grafting or impregnation) [13]. Much effort has been devoted to the incorporation of aluminum into SBA-15 to create acidic sites and improve its hydrothermal stability, which is also an important characteristic of the material if used as a catalyst support. It is extremely difficult to directly introduce metals into the siliceous skeleton of SBA-15, because under strong acidic synthesis conditions (pH < 2), metals exist only in their cationic form rather than their corresponding oxo species [14–16]. Therefore, much work in the past was devoted to postsynthesis grafting. Nevertheless, introduction of heteroatoms into the siliceous skeleton of SBA-15 in such a way has some drawbacks, such as pore blockage and texture property reduction [17,18]. Previous studies

* Corresponding authors. Addresses: Department of Chemistry and Shanghai Key Laboratory of Molecular Catalysis and Innovative Materials, Fudan University, Shanghai 200433, People's Republic of China (C. Yu), State Key Laboratory of Heavy Oil Processing, China University of Petroleum, Changping, Beijing 102249, People's Republic of China. Fax: +86 10 89734836 (X. Bao).
E-mail addresses: czyu@fudan.edu.cn (C. Yu), baoxj@cup.edu.cn (X. Bao).

0021-9517/$ - see front matter © 2011 Elsevier Inc. All rights reserved.
doi:10.1016/j.jcat.2011.10.023

also demonstrated that the introduction of excessive Al may decrease the mesostructure regularity and the hydrothermal stability [19,20].

Until now, there have been few reports on the synthesis of ordered mesoporous Al-SBA-15 with both strong acidity and high hydrothermal stability under high-temperature steaming conditions. To address this issue, we report a novel synthesis approach. Our synthesis relies on fundamental understanding of the postsynthesis grafting process. To favor the formation of Si–O–Al bonds, the key is to maximize both Si–OH and Al–OH concentrations, which can be achieved by adjusting the pH during the high-temperature hydrothermal treatment (HTHT) process [21]. Our approach has the following features: (1) The HTHT pH is chosen near the isoelectric point (pI) of silica (pI $\sim$ 2) to produce a large amount of Si–OH for postgrafting [15,22]; (2) the HTHT is advantageous for the endothermic hydrolysis reaction and thus can transform more Al^{3+} into Al–OH species and benefit the formation of hydrothermally stable mesoporous materials; (3) the preformation of as-synthesized pure silica, SBA-15, at first and then the postgrafting of Al species are essential to maintain a highly ordered mesostructure with uniform mesopores. By maintaining the HTHT pH at its optimum value, 2.4, Al-SBA-15 with a molar Si/Al ratio (φ) of 5.1 similar to that of the initial gel mixture and homogenously distributed Al species in the walls was successfully obtained. Significantly, the material showed high hydrothermal stability after the steaming treatment at 800 °C for 5 h and relatively strong acidity. As expected, the NiW catalyst supported on Al-SBA-15 with high accessibility and enhanced B and L acidities demonstrated outstanding advantages for DBT HDS over the NiW catalysts supported on SBA-15 and γ-Al_2O_3.

2. Experimental

2.1. Synthesis of Al-SBA-15 and SBA-15

Triblock copolymer P123 ($EO_{20}PO_{70}EO_{20}$, M_w = 5800) was purchased from Aldrich. Tetraethyl orthosilicate (TEOS), aluminum nitrate ($Al(NO_3)_3$), hydrochloric acid (HCl), and acetic acid (HAc) were obtained from Shanghai Chemical Co., People's Republic of China. The synthesis procedure is shown in Fig. 1. In a typical synthesis batch, 3 g of P123 and 4.66 g of HAc were dissolved in 80 mL of a 2.0-M HCl aqueous solution, followed by the addition of 6.24 g of TEOS under stirring. After being stirred at 38 °C for 24 h, the resulting white precipitate was filtered. The product was mixed with 60 g of deionized water containing a required amount of $Al(NO_3)_3$, and the pH value of the solution was adjusted from 1 to 4 using a 2.0-M HCl solution. After being stirred for 2 h at room temperature, the mixture was transferred into an autoclave for HTHT at 150 °C for 24 h. The final product was collected by filtration, washed with deionized water, dried in air, and calcined at 550 °C to remove the template. The synthesized samples under different conditions were named S-5-*X*, where S is the abbreviation of the sample, 5 denotes the molar Si/Al ratio in the initial synthesis mixture, and *X* stands for the pH value of the hydrothermal treatment solution.

For comparison, a SBA-15 sample was also prepared as follows: 3 g of P123 and 4.66 g of HAc were dissolved in 80 mL of a 2.0-M HCl aqueous solution, followed by the addition of 6.24 g of TEOS under stirring. After being stirred at 38 °C for 24 h, the resulting white precipitate was directly transferred into an autoclave for HTHT at 150 °C for 24 h, and the final product was collected by filtration, washed with deionized water, dried in air, and calcined at 550 °C to remove the template.

2.2. Preparation of Al-SBA-15, SBA-15, and γ-Al_2O_3 supported NiW HDS catalysts

A NiW/Al-SBA-15 catalyst (the sample S-5-2.4 was selected as the support because of its high aluminum loading and high hydrothermal stability) and a NiW/SBA-15 catalyst were prepared by the sequential pore volume impregnation method using ammonium metatungstate and nickel nitrate (both of which were purchased from Beijing Chemical Co., People's Republic of China) as metal precursors, with W impregnated in the first and Ni in the second. During the impregnation of W and Ni, the metal precursors were dissolved with a 0.5-M oxalic acid (Shanghai Chemical Co., People's Republic China) solution. The oxalic acid can preferentially remove the extraframework Al species formed during the calcination step and thus reopen the blocked pore channels of the Al-SBA-15 [23]. After each of the above impregnation steps, the sample was dried at 120 °C for 2 h and calcined at 500 °C for 4 h. The theoretical loadings of NiO and WO_3 in the SBA-15 and Al-SBA-15 supported catalysts were 2.6 and 23 wt.% [24], respectively. For comparison, a commercial NiW/γ-Al_2O_3 (Crosfield Sphexicat 550 s) [25] catalyst was also prepared in a similar way to that for the NiW/Al-SBA-15 catalyst; the theoretical loadings of NiO and WO_3 for the NiW/γ-Al_2O_3 catalyst were 4 and 22 wt.%, respectively.

2.3. Characterizations

The supports and catalysts were characterized by X-ray fluorescence spectroscopy (XRF), X-ray powder diffraction (XRD), N_2 adsorption–desorption, temperature-programmed desorption of ammonia (NH_3-TPD), temperature-programmed reduction with hydrogen (H_2-TPR), Fourier transformed infrared (IR) spectroscopy with pyridine adsorption (pyridine-FTIR), ^{27}Al nuclear magnetic resonance (^{27}Al NMR) spectroscopy, and high-resolution transmission electron microscopy (HRTEM).

The NiO and WO_3 contents of the catalysts were determined by XRF conducted on a Rigaku ZSX-100e instrument. XRD patterns were recorded on a Siemens D5000 diffractometer, using Cu Kα radiation (λ = 1.5406 Å) and with 2θ scanning speed at 4°/min and diffraction lines of 2θ between 15° and 60°. Low-angle XRD

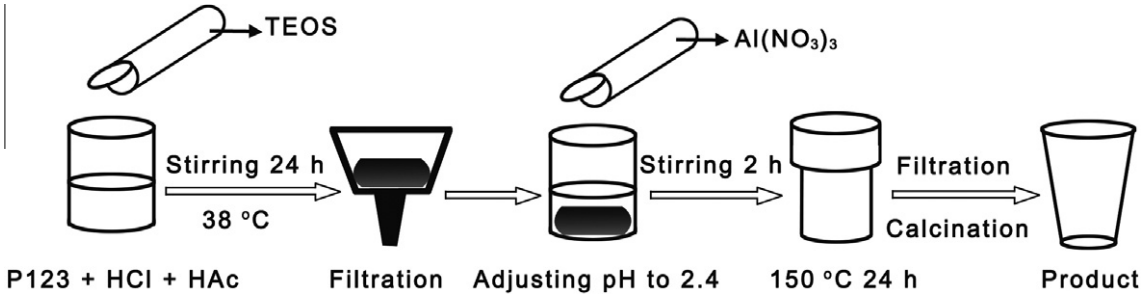

Fig. 1. An optimized procedure for the synthesis of Al-SBA-15.

(2θ = 0.65–5°) analyses were performed on a Bruker D8 Advance diffractometer using small divergence and a scattering slit of 0.05°.

N_2 adsorption–desorption measurements of the supports and corresponding catalysts were performed on a Micromeritics ASAP 2002 instrument. The samples to be measured were first degassed in the preparation station at 250 °C under a vacuum of 10^{-5} Torr for 15 h, and then switched to the analysis station for adsorption–desorption at liquid nitrogen temperature. The specific surface areas were calculated by the Brunauer–Emmett–Teller (BET) method [26], and the pore volumes of the samples were calculated from N_2 adsorption–desorption isotherms. The mesopore diameters corresponding to the maxima of the pore size distributions were obtained from desorption isotherms by the Barret–Joyner–Halenda (BJH) method [27].

^{27}Al NMR experiments on Al-SBA-15 were performed on a Varian Unity Inova 300 spectrometer (Varian, USA) equipped with a double-resonance 6-mm Chemagnetics MAS probe and operated at frequency 59.59 MHz, pulse width 1.5 μs, radiofrequency field strength 50 G, pulse delay 2 s, and spinning rate 5 kHz for 10,000 scans.

H_2-TPR analyses of the oxidic catalysts were performed on a home-built apparatus. First, the catalyst samples, each 100 mg, were pretreated in an Ar stream at 450 °C for 2 h and then cooled to room temperature. Then, the Ar flow was switched to a 10% H_2/Ar flow, and the catalyst samples were heated to 1050 °C at a rate of 10 °C min^{-1} and kept at this temperature for 0.5 h. The H_2 consumption for reducing the corresponding metal oxides in the catalysts was detected by a thermal conductivity detector (TCD).

The acid strength of the supports, oxidic and sulfided catalysts NiW/SBA-15, NiW/Al-SBA-15, and NiW/γ-Al_2O_3, was determined by NH_3-TPD measurements using the same apparatus described for the H_2-TPR experiments. First, the samples, each 100 mg, were heated from room temperature to 600 °C at a rate of 10 °C min^{-1} and then cooled to 100 °C in a pure He flow. Then, ammonia was adsorbed at 100 °C for 20 min, and subsequently the samples were purged by a flowing He stream at 100 °C for 1 h to remove excessive and physically adsorbed NH_3. Finally, the samples were heated from 100 to 600 °C at a rate of 10 °C min^{-1} in a pure He flow and desorption patterns were recorded. The sulfided catalysts were obtained by sulfiding the corresponding oxidic catalysts with a 3 wt.% CS_2/cyclohexane mixture at 400 °C and 4 MPa for 4 h.

Pyridine adsorption experiments were conducted on self-supported wafers in an in situ FTIR cell. The samples were dehydrated at 500 °C for 5 h under a vacuum of 1.33×10^{-3} Pa and the adsorption of pure pyridine vapor at room temperature for 20 min was followed; then the system was evacuated at 200 and at 350 °C, and finally FTIR spectra were recorded.

HRTEM images of Al-SBA-15 and the sulfided catalysts NiW/SBA-15, NiW/Al-SBA-15, and NiW/γ-Al_2O_3 were obtained on a Philips Tecnai G2 F20 transmission electron microscope operated at an accelerating voltage of 200 kV.

2.4. Hydrothermal stability evaluation

The high-temperature hydrothermal stability of the calcined samples was tested by treating samples at 800 °C for 5 h in a 15% steam/nitrogen stream with the flow rate of nitrogen at 45 mL min^{-1}.

2.5. HDS performance assessment

The DBT HDS activity of the NiW/Al-SBA-15, NiW/SBA-15, and NiW/γ-Al_2O_3 catalysts was assessed in a fixed-bed microreactor using 1 wt.% DBT in heptane as a model compound. Before the reaction, the catalyst (0.5 g) to be tested was presulfided for 4 h at 360 °C, total pressure of 4.0 MPa, and a volumetric H_2/hydrocarbon (HC, 3 wt.% CS_2 in heptane) ratio of 300. The HDS reaction was carried out under conditions of temperature 360 °C, weight hourly space velocity (WHSV) 30 h^{-1}, total pressure 4.0 MPa, and volumetric H_2/HC ratio 300. After steady state was reached, the liquid product was collected, and the sulfur content in the reactant and product was analyzed by a WK-2C microcoulombmeter (Jiangsu Jiangfen Electroanalytical Instrument Co., People's Republic of China). The various DBT HDS reaction products were analyzed by an offline Finnigan Trace GC/MS instrument installed with an HP-5MS capillary column (30 m × 0.25 mm × 0.25 μm) and a pulsed flame photometric detector (PFPD). Under the operating conditions tested, DBT was converted to biphenyl (BP) and cyclohexylbenzene (CHB). Moreover, the further hydrogenation and isomerization products, such as cyclopentylmethylbenzene (CPMB), cyclopentylcyclohexyl (CPCH), and cyclopentylmethylcyclohexane (CPMCH), were also detected from the products obtained over the NiW/Al-SBA-15 catalyst. The DBT HDS reaction of the NiW/Al-SBA-15 catalyst was also conducted at other temperatures, such as 320, 340, and 380 °C, to determine how the reaction temperature influences the selectivity for the various DBT HDS products.

Catalyst activity was determined according to the following equation by considering DBT HDS as a pseudo-first-order reaction [28],

$$k = \frac{F}{m} \ln\left(\frac{1}{1-\tau}\right), \tag{1}$$

where F is the feeding rate of the reactant in mol h^{-1}, m is the catalyst mass in g, and τ is the total conversion of DBT. In addition, the DBT HDS rate was also calculated in terms of turnover frequency, TOF (s^{-1}), defined as the number of desulfurized DBT molecules per second and per catalytic site (per W atom on the edges of per WS_2 crystallite). Thus-defined TOF represents the HDS efficiency of the W phase promoted by Ni (Ni–W–S) in view of the negligible HDS ability of the single promoter phase with a minor amount. For supported WS_2 or MoS_2 HDS catalysts, Eq. (2), which is widely used to estimate the relative proportion of W atoms on the edges versus the total number of W atoms per crystallite, can be recommended as a good estimate of TOF [28,29],

$$\frac{W_{edge}}{W_{total}} = \frac{\sum_{i=1}^{t}(6n_i - 6)}{\sum_{i=1}^{t}(3n_i^2 - 3n_i + 1)}, \tag{2}$$

where W_{edge} is the total number of W atoms located on the edges, W_{total} is the total number of W atoms, n_i is the number of W atoms along one edge of a WS_2 slab determined from its length ($L = 3.2(2n_i - 1)$Å), and t is the total number of slabs determined by HRTEM observation. Here, it is assumed that all the edge sites are active for HDS reactions, so the real value of TOF could be higher than that estimated from Eq. (2).

To understand whether the incorporation of Al into SBA-15 can enhance the HDS reaction stability of the NiW/Al-SBA-15 catalyst, the HDS behavior of the NiW/Al-SBA-15 catalyst was also evaluated using a fluid catalytic cracking (FCC) diesel sampled from a Chinese refinery with its boiling point in the range from 201 to 412 °C, a density of 0.8762 g cm^{-3}, and a sulfur content of 1880 ppm. The HDS reaction was conducted in the same fixed-bed microreactor used for the DBT HDS. Before being loaded into the reactor, 2 mL of the catalyst to be tested was diluted with the same volume of quartz particles. The NiW/Al-SBA-15 catalyst was sulfided in a mixture of 3 wt.% CS_2 in cyclohexane. The sulfidation procedure comprised the following steps: (1) The sulfiding feed was introduced to wet the catalyst bed at 150 °C and 6 MPa, after which the bed temperature was linearly increased to 180 °C at a rate of 60 °C/h and kept at this temperature for 0.5 h; (2) the bed temperature was increased to 230 °C at a rate of 60 °C/h and

maintained there for 2 h; (3) the bed temperature was increased to 280 °C at the same rate and maintained there for 0.5 h; and (4) the bed temperature was increased to the final sulfidation temperature 360 °C, and the operation was stabilized for 3 h. After sulfidation, the feeding flow was switched to the diesel feed, and the HDS assessment was carried out. The operating conditions were WHSV 1.5 h^{-1}, temperature 360 °C, total pressure 6 MPa, and volumetric H_2/oil ratio 500. After steady state was achieved, the liquid product was sampled for analysis.

3. Results and discussion

3.1. Characterization results for the supports

Fig. 2 shows the XRD patterns of calcined Al-SBA-15 samples with a molar Si/Al ratio (φ) of 5. All of the Al-SBA-15 samples exhibit three well-resolved diffraction peaks indexed as (100), (110), and (200) that are associated with the *p6mm* hexagonal symmetry, indicating that highly ordered mesoporous Al-SBA-15 materials have been successfully synthesized at a temperature as high as 150 °C when the pH value (*X*) of the hydrothermal treatment solution is in the range 1–4. It is also noted that the variation of *X* has little influence on the cell parameter of S-5-*X* calculated from the first reflection peak shown in Fig. 2. The values of φ calculated from the XRF analysis results as a function of the HTHT pH for S-5-*X* are displayed in Fig. 3. The results show that the experimentally determined φ of sample S-5-2.4 is exactly equal to the expected φ value (5). For the group S-5-*X*, φ decreases rapidly when *X* is increased from 1.0 to 2.4, and then increases gradually until *X* is 4. The point *X* = 2.4 is a turning point, where φ reaches its minimum, which is 5.1 for S-5-2.4. It is noteworthy that the measured φ at *X* = 2.4 is just slightly higher than 5, indicating that almost all Al species added in the initial reaction mixture have been introduced into the final products.

Considering the grafting reactions between Si–OH and Al–OH described by Eqs. (3) and (4), it is found that to maximize both Si–OH and Al–OH concentrations the key is to adjust the hydrothermal treatment pH value:

$$[Al(H_2O)_6]^{3+} \rightarrow [Al(OH)_x(H_2O)_{6-x}]^{3-x} + xH^+ \quad (3)$$

$$Si - OH + HO - Al \rightarrow Si - O - Al + H_2O. \quad (4)$$

Before the hydrothermal treatment, the ordered mesostructured SBA-15-type material with abundant silanol groups in its mesoporous walls has already been formed. During the subsequent HTHT process, the silica matrix experiences further wall condensation and framework shrinkage. When the HTHT pH is lower than 2.4, the relatively high acidity of the solution inhibits the hydrolysis reaction of Al species; thus most Al species are homogeneously dispersed in the synthesis system in the form of Al^{3+} cations, as shown in Eq. (3). Consequently, with decreasing pH, the amount of aluminum grafted into the final samples decreases rapidly. When the HTHT pH is near the isoelectric point of silica (pI ~ 2) [22], the further condensation of silica during the HTHT is slowest,

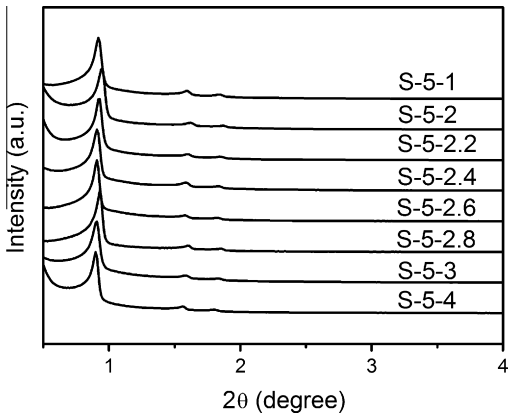

Fig. 2. Low-angle XRD patterns of samples S-5-*X* calcined at 550 °C.

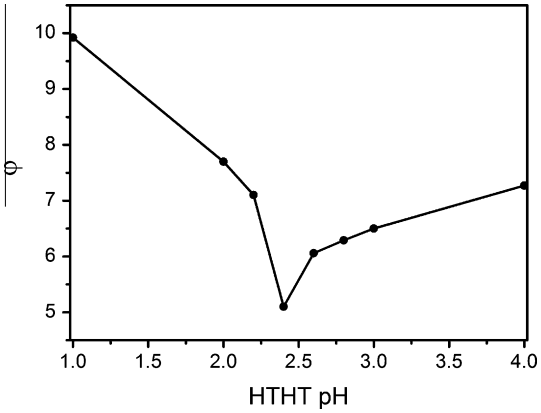

Fig. 3. φ as a function of the HTHT pH for calcined samples S-5-*X*.

and most Al species are in the form of aluminum oxo species rather than Al^{3+} cations, leading to silica walls with the highest silanol concentration where almost all aluminum oxo species are grafted into mesoporous walls. On the other hand, when the HTHT pH is increased, the value of φ shows a changing trend similar to the case pH < 2.4, because the further condensed silica walls decrease silanol concentration and thus lead to less aluminum being grafted into the mesoporous framework and a gradually increasing φ of the final samples. As a result, the silanol concentration of pure silica samples hydrothermally treated at a pH value close to pI reaches its maximum when the other synthesis conditions are the same [21]. We conclude that highly ordered mesoporous materials with a relatively large amount of grafted aluminum can be obtained at a HTHT pH of 2.4. So we hereafter choose the sample S-5-2.4 for more detailed study and denote it as Al-SBA-15.

The textural and structural characteristics of the synthesized Al-SBA-15 and SBA-15 are given in Table 1. The results show that the

Table 1
Textural and structural characteristics of Al-SBA-15 and SBA-15.

Sample	φ[a]	S_{BET} ($m^2\ g^{-1}$)	V_p ($cm^3\ g^{-1}$)[b]	D_p (Å)[c]
Calcined Al-SBA-15	5.1	368	0.8	69
Calcined Al-SBA-15 after steaming for 5 h	5.1	312	0.7	60
Calcined SBA-15	/	389	1.0	83
Calcined SBA-15 after steaming for 5 h	/	217	0.5	42

[a] Molar Si/Al ratio determined by XRF.
[b] Pore volume.
[c] Pore diameter determined from the desorption isotherms by the BJH method.

BET surface area and pore volume of the calcined Al-SBA-15 are slightly smaller than those of the calcined SBA-15, decreasing from 389 to 368 $m^2 g^{-1}$ and from 1.0 to 0.8 $cm^3 g^{-1}$, respectively, indicating that the grafting treatment and calcination cause slight blockage of mesopores. Moreover, the drop in pore diameter (D_p) from 83 Å for SBA-15 to 69 Å for Al-SBA-15 indicates that part of the extraframework Al species are located inside the pores of the Al-SBA-15 material [7]. After the steaming treatment at 800 °C for 5 h, the decreases in BET surface area and total pore volume were 15.2% and 12.7% for Al-SBA-15; they were 44.2% and 49.4% for SBA-15, respectively. For comparison, the sample 1.5% Al-MUS-S prepared by using preformed zeolite seeds as precursors exhibited larger decreases in BET surface area and total pore volume, 21.3% and 56.6% [30].

The N_2 adsorption–desorption isotherms of the calcined Al-SBA-15 before and after steaming treatment at 800 °C for 5 h are shown in Fig. 4A. The calcined Al-SBA-15 exhibits a typical type IV isotherm and a very steep capillary condensation step accompanied at relative pressure P/P_0 ranging from 0.65 to 0.90, characteristic of ordered mesoporous materials with large and uniform mesopores. The dimension and uniformity of mesopores in the calcined Al-SBA-15 before and after steaming treatment are also directly reflected by the pore size distribution curves. From the inset of Fig. 4A, it can be seen that the calcined Al-SBA-15 possesses a relatively narrower pore size distribution, which is typical of a well-ordered mesostructured material. It is worthy of noting that only slight changes are observed in the N_2 adsorption–desorption isotherm and pore size distribution curve of the calcined Al-SBA-15 after treatment with steam at 800 °C for 5 h. In addition, after the steaming treatment, Al-SBA-15 still displays three well-resolved peaks, indexed as the (100), (110), and (200) diffractions of a highly ordered hexagonal symmetry (Fig. 4B).

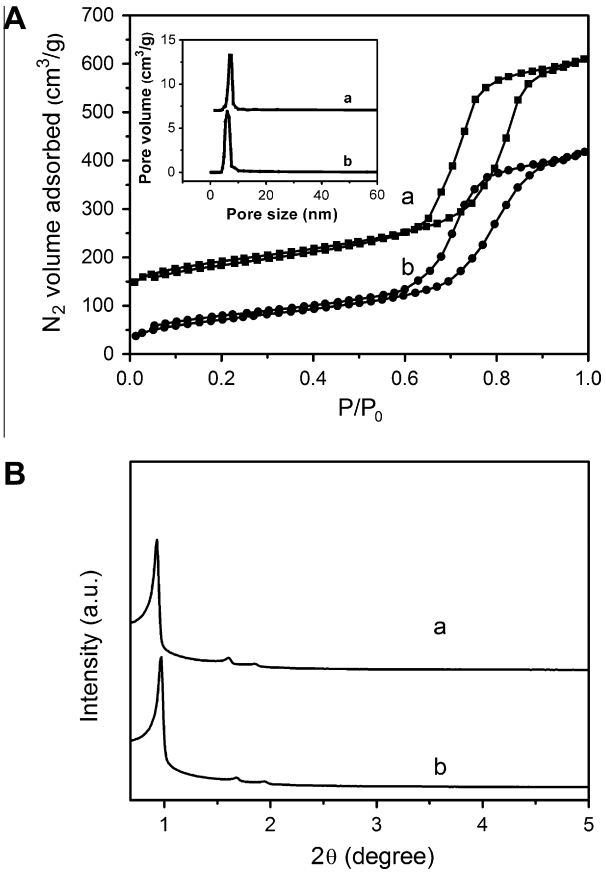

Fig. 4. N_2 adsorption–desorption isotherms and pore size distribution curves (A) and low-angle XRD patterns (B) of Al-SBA-15 calcined (a) and steamed at 800 °C for 5 h (b).

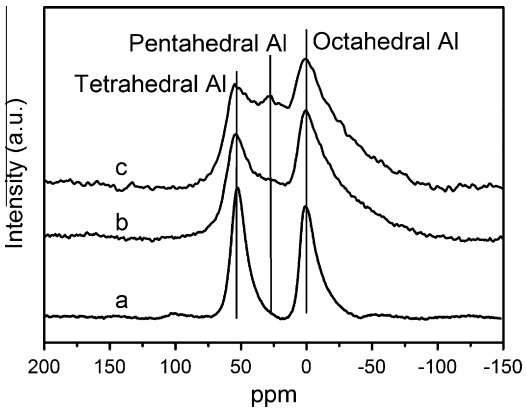

Fig. 5. ^{27}Al NMR spectra of Al-SBA-15 (a), calcined Al-SBA-15 (b), and steamed Al-SBA-15 (c).

The ^{27}Al NMR spectra (Fig. 5a) of the as-synthesized Al-SBA-15 show that large amounts of Al species have been introduced into SBA-15; significantly, the introduced Al species are inclined to locate at 4-coordinated sites (53 ppm) [30]. The deconvolution of the spectra shows that the ratio of 4-coordinated framework Al to 6-coordinated (0 ppm) extraframework Al is 1.7, suggesting that about 63% of aluminum atoms incorporated into Al-SBA-15 are in the silica framework, while the other extraframework aluminum may be located on the surface of Al-SBA-15. For Al-SBA-15 prepared by direct synthesis or postsynthesis methods [9,31–33], the initial molar Si/Al ratio of the materials is usually between 30 and 40, which results in maximum alumina loadings of 2.1 and 2.8 wt.%, respectively. When the alumina loading is higher than 14 wt.%, it is difficult to introduce all of the aluminum into the framework, with part of the aluminum species in the resulting materials being 6-coordinated extraframework aluminum. After calcination at 550 °C to remove the template, more octahedral Al species, accompanied by a small amount of pentahedral Al species (27 ppm) [34], are observed in the corresponding calcined Al-SBA-15 (Fig. 5b), indicating that calcination at high temperature causes the "flaking-off" of Al atoms from tetrahedral sites in the mesoporous walls to octahedral and pentahedral sites. This phenomenon is more obvious when the thermal treatment temperature is increased to 800 °C under steaming conditions (Fig. 5c), for which the deconvolution of the ^{27}Al NMR spectra reveals that the ratio of 4-coordinated Al to 5-coordinated Al to 6-coordinated Al is 2.1:1:4.6.

The above discussion raises the question of where the extraframework Al is located. To answer this question, wide-range XRD and HRTEM characterizations were conducted and results are shown in Figs. 6 and 7. In the patterns of the Al-SBA-15 and calcined Al-SBA-15, there are no characteristic reflections associated with γ-Al_2O_3, indicating no bulky γ-Al_2O_3 aggregates on Al-SBA-15. The HRTEM images of the Al-SBA-15 and calcined Al-SBA-15 show that Al-SBA-15 has well-ordered hexagonal arrays of mesopores and a 2D *p6mm* hexagonal structure; its large pores (~7 nm) are clearly visible, indicating no obvious pore blockage of the Al-SBA-15. The absence of the signals representing alumina in the wide-range XRD and HRTEM characterization results of Al-SBA-15 suggests that the extraframework aluminum is homogeneously distributed on the outer surface and in the mesopores of Al-SBA-15.

To evaluate the strength and types of acid sites of the calcined Al-SBA-15 before and after the steaming treatment at 800 °C for

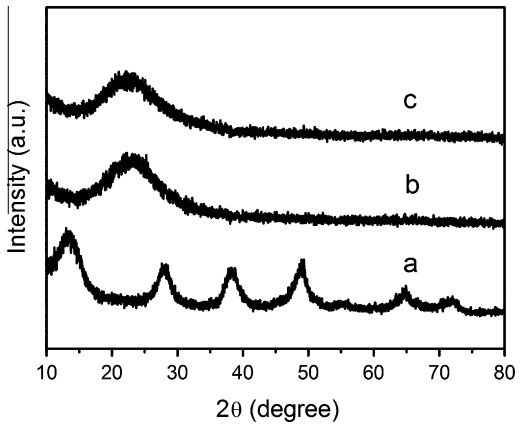

Fig. 6. Wide-angle XRD patterns of γ-Al_2O_3 (a), Al-SBA-15 (b), and calcined Al-SBA-15 (c).

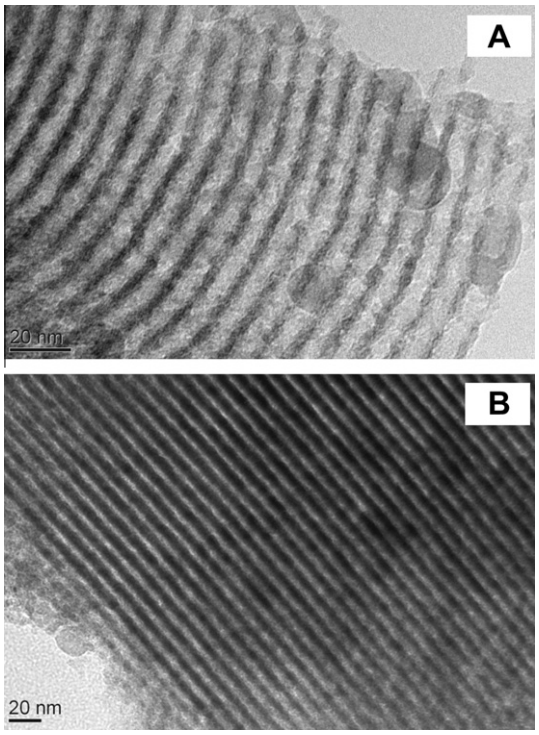

Fig. 7. HRTEM images of Al-SBA-15 (A) and calcined Al-SBA-15 (B).

5 h, pyridine adsorption IR spectroscopy measurements were taken after evacuation at 200 and 350 °C in the wavenumber range 1600–1400 cm^{-1} and the results are shown in Fig. 8. It can be seen that in the spectra of the calcined Al-SBA-15 (Fig. 8A), there are three sharp bands due to the C–C stretching vibrations of pyridine. According to the literature [35], the strong band at 1491 cm^{-1} is due to pyridine molecules adsorbed onto both B and L acid sites, while the bands at 1543 and 1454 cm^{-1} are due to protonation of pyridine molecules by B acid sites and pyridine molecules adsorbed onto L acid sites. After degassing at 350 °C, all the bands still exist, indicating that the calcined Al-SBA-15 has medium/strong acidity. We can assume that Al incorporation into SBA-15 can generate bridging hydroxyl groups (Si–OH–Al, B acid sites) on Al-SBA-15 [14]. These results are well in line with the ^{27}Al NMR observations of framework Al species. Similar results can be also seen for Al-SBA-15 after steaming treatment at 800 °C for 5 h. Fig. 8B reveals that steamed Al-SBA-15 still shows the obvious

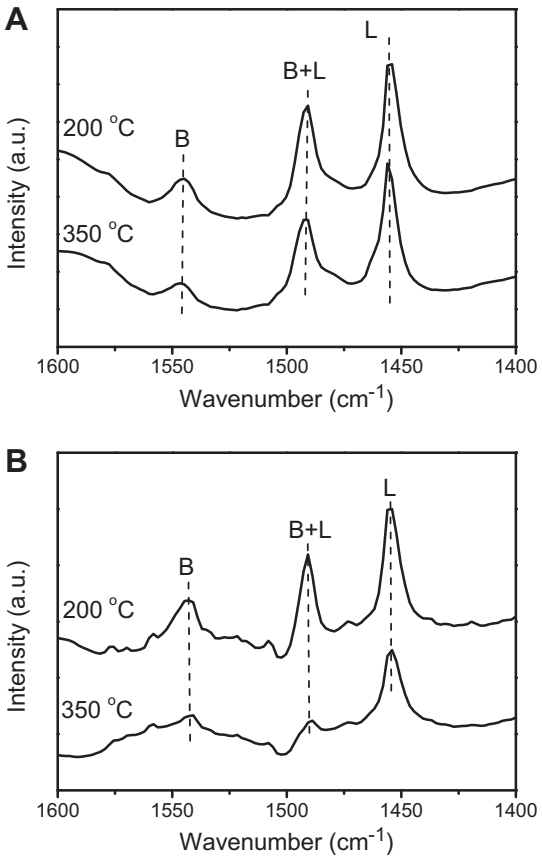

Fig. 8. Pyridine-FTIR spectra of Al-SBA-15 calcined only (A) and calcined first and then steamed at 800 °C for 5 h (B) after degassing at 200 and 350 °C.

bands at 1543 and 1454 cm^{-1} after degassing at 200 °C, indicating that the steamed Al-SBA-15 possesses both B and L acid sites. However, after degassing at 350 °C, the band at 1543 cm^{-1} becomes indiscernible due to the dealumination of the mesoporous framework during the high-temperature steaming treatment.

In summary, the foregoing results demonstrate that Al-SBA-15 with the characteristic hexagonal mesoporous structure of SBA-15 has been successfully prepared at pH 2.4. Compared with previous studies [9,31–33], the Al-SBA-15 we have synthesized has a much lower molar Si/Al ratio (φ = 5.1, equivalent to about 14.3 wt.% alumina loading), extremely high hydrothermal stability, and moderate B/L acidity. The ^{27}Al NMR measurements confirm that most aluminum species in the initial synthesis system have been incorporated into the SBA-15 silica framework and homogenously distributed in the walls. In line with this, the pyridine adsorption IR spectroscopy measurements indicate that thus prepared Al-SBA-15 possesses both moderate B and L acidity.

3.2. Characterization results of the catalysts

The textural characteristics of the three supported NiW catalysts are given in Table 2. It is noted that after being loaded with the active metals Ni and W, catalysts NiW/SBA-15 and NiW/Al-SBA-15 suffer a decrease in surface area by 33% and 26%, respectively, partly due to the increase in their densities. Compared with that of Al-SBA-15, the decreased pore diameter of NiW/Al-SBA-15 is due to the incorporation of Ni and W into mesopores [36]. Fig. 9A shows the low-angle XRD patterns of NiW/Al-SBA-15 and NiW/SBA-15 catalysts. The three reflections characteristic of the hexagonal structure are still present, indicating the highly ordered

Table 2
Compositions and textural characteristics of the catalysts.

Sample	SiO_2 (wt.%)[a]	Al_2O_3 (wt.%)[a]	φ[b]	NiO (wt.%)[a]	W_xO_y (wt.%)[a]	S_{BET} ($m^2\ g^{-1}$)	V_p ($cm^3\ g^{-1}$)	D_p (Å)[c]
NiW/Al-SBA-15	63.1	8.6	6.2	3.2	24.5	273	0.5	65
NiW/SBA-15	72.2	–	–	3.2	24.4	261	0.7	82
NiW/γ-Al_2O_3	–	73.6	–	4.1	22.3	230	0.5	48

[a] Determined by XRF.
[b] Molar Si/Al ratio.
[c] Pore diameter determined from the desorption isotherms by the BJH method.

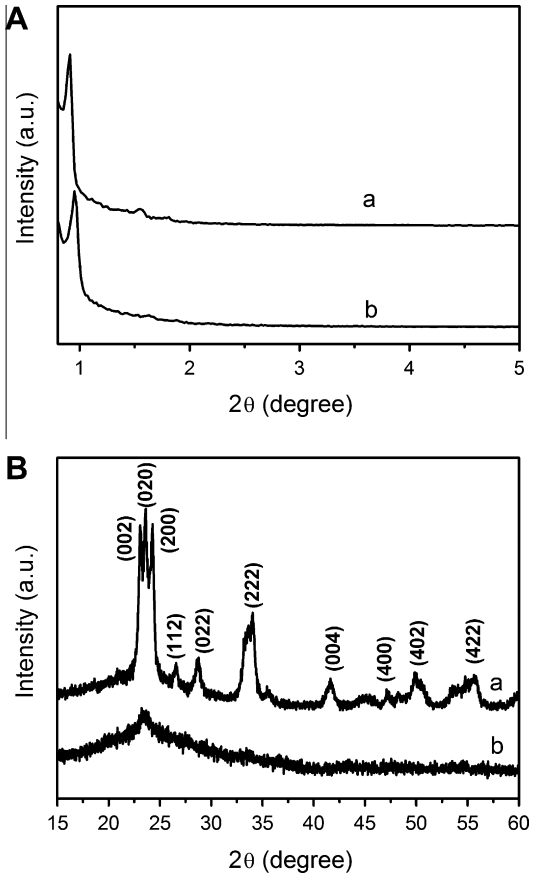

Fig. 9. The low- (A) and wide-angle (B) XRD patterns of NiW/SBA-15 (a) and NiW/Al-SBA-15 (b). In (B), the 10 peaks of NiW/SBA-15 are indexed as the characteristic reflections associated with monoclinic WO_3 crystallites.

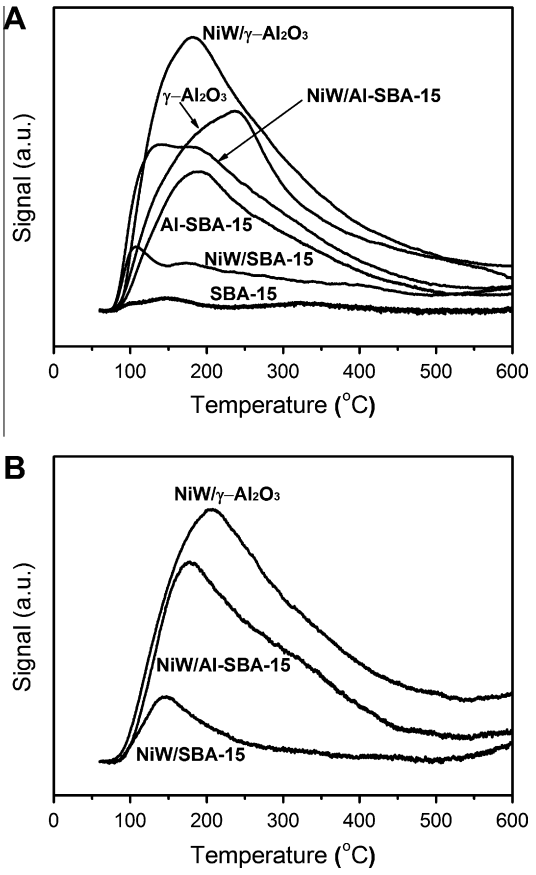

Fig. 10. NH_3-TPD profiles of the supports and oxidic catalysts (A) and the sulfided catalysts (B).

mesostructure preservation of the supports after they are loaded with Ni and W. The wide-angle XRD characterization (Fig. 9B) demonstrates that only the catalyst supported on the pure SBA-15 displays the characteristic reflections associated with monoclinic WO_3 crystallites (JCPDS Card 83-0951s), signifying that the incorporation of aluminum into the SBA-15 support improves the dispersion of W species. This can be reasonably explained by the fact that the incorporation of aluminum to SBA-15, especially the extraframework aluminum species, could play a beneficial role in creating the "highly reactive" Al–OH responsible for the stronger metal–support interaction, leading to the better dispersion of W species.

The acidity of the three supports and the corresponding oxidic and sulfided catalysts was studied by two methods. The first method used was NH_3-TPD measurement. In terms of desorption temperature, acid sites are classified as weak (100–250 °C), medium (250–400 °C), and strong (>400 °C). The NH_3-TPD profiles of the three catalysts are shown in Fig. 10A. Both the NiW/SBA-15 and NiW/Al-SBA-15 catalysts show two desorption peaks at about 100 and 175 °C, corresponding to weak acidic sites arising from surface hydroxyl groups attached to Si [37]. The NiW/Al-SBA-15 and NiW/γ-Al_2O_3 catalysts display a similar broad peak in the temperature range from 75 to 400 °C, revealing the presence of both weak and medium acid sites. Moreover, the intensity of the desorption peaks shows that the number of total acid sites in the NiW/SBA-15 catalyst is much lower than that in the NiW/Al-SBA-15 and NiW/γ-Al_2O_3 catalysts. NH_3-TPD characterization of the three sulfided catalysts was also conducted and the results are shown in Fig. 10B. Li et al. [38] did the NH_3-TPD characterization of the oxidic and sulfided catalysts, and they considered that the sulfidation did not change the acidic structures dramatically. From Fig. 10, we can see that the amounts of acidity for the oxidic and sulfided catalysts increase in the same order, NiW/SBA-15 < NiW/Al-SBA-15 < NiW/γ-Al_2O_3.

To further determine the strength and types of acid sites in the three catalysts, pyridine adsorption IR spectroscopy measurements

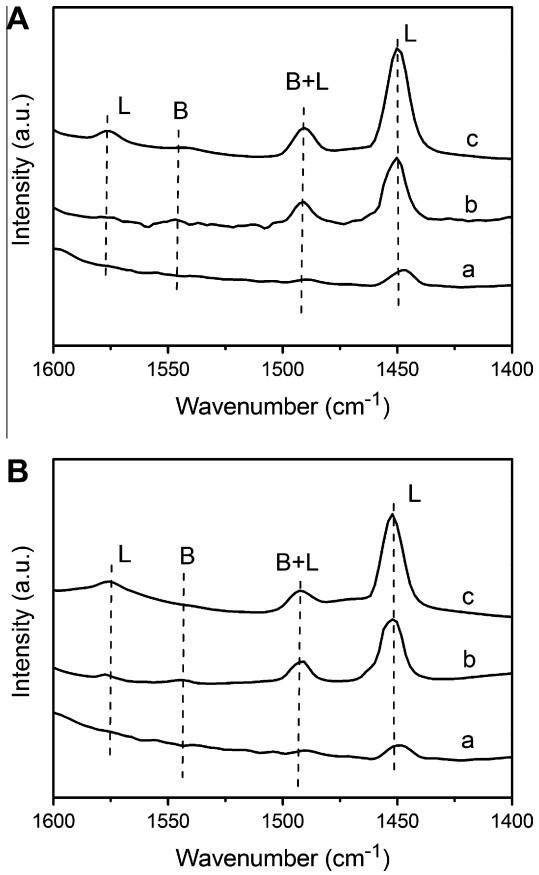

Fig. 11. Pyridine-FTIR spectra of NiW/SBA-15 (a), NiW/Al-SBA-15 (b), and NiW/γ-Al_2O_3 (c) after degassing at (A) 200 and (B) 350 °C.

were taken after evacuation at 200 and 350 °C in the wavenumber range 1600–1400 cm^{-1} and the results are shown in Fig. 11. The peaks at 1446 and 1577 cm^{-1} are attributed to pyridine adsorbed onto L acid sites, and the peak at 1546 cm^{-1} is assigned to pyridine adsorbed onto B acid sites, while the peak at 1490 cm^{-1} is ascribed to pyridine adsorbed onto both B and L acid sites. An attempt has also been made to quantitatively estimate the number of B and L acid sites for the three catalysts using pyridine adsorption followed by degassing at 200 and 350 °C, corresponding to the total and medium/strong acid sites. The acid strength distributions and acid quantities of the supports and corresponding catalysts are listed in Table 3. After degassing at 200 °C, the total amount of (B + L) acid sites of the NiW/Al-SBA-15 catalyst is slightly lower than that of the NiW/γ-Al_2O_3 catalyst, but is about 4.7 times that of the NiW/SBA-15 catalyst. This difference is more notable (about six times) for the amounts of medium and strong acid sites (B + L after degassing at 350 °C). The NiW/Al-SBA-15 catalyst possesses more B acid sites, especially medium/strong B acid sites, than the NiW/γ-Al_2O_3 catalyst. Compared with the support Al-SBA-15, the NiW/Al-SBA-15 catalyst has more L acid sites but fewer B acid sites. This is because (1) during the two impregnation steps, the acidic solutions would react with the Al species, leading to the loss of Al species (the values of φ for the Al-SBA-15 support and the NiW/Al-SBA-15 catalyst are 5.1 and 6.2, respectively); and (2) after the impregnation of W and Ni species, the two following calcination steps at high temperature would cause the "flaking off" of Al atoms from tetrahedral sites (framework) in the mesoporous walls to pentahedral sites and octahedral sites (extraframework, with the nature of weak L acid) [39]. In the NiW/SBA-15 and NiW/γ-Al_2O_3 catalysts, there exist more L acid sites than in the SBA-15 and γ-Al_2O_3 supports, due to the formation of Si–O–W and Al–O–W linkages on the surfaces of the catalysts [14]. Pyridine adsorption IR spectroscopy measurements of the sulfided catalysts were also conducted after evacuation at 200 and 350 °C in the wavenumber range 1600–1400 cm^{-1} (see Fig. S1 in the Supplementary Information). It is observed that both sulfided NiW/Al-SBA-15 and NiW/γ-Al_2O_3 have B and L acid sites, while the sulfided NiW/SBA-15 has only a negligible number of L acid sites. The numbers of acid sites for all the three sulfided catalysts are lower than those for the oxidic catalysts (see Table S2 in the Supplementary Information).

Strong interaction usually leads to good dispersion of metal oxides and benefits the creation of accessible active sites [40], while weak interaction yields metal oxides that can easily be reduced/sulfided but gives rise to the formation of larger active particles and thus poorer dispersion of active species [41]. For WO_3 species dispersed on a support, octahedrally coordinated WO_x species are reduced at temperatures from 300 to 700 °C, while tetrahedrally coordinated or dimeric WO_x species with strong interaction with supports such as Al_2O_3 are more difficult to reduce, requiring a temperature of around 900–1000 °C [24]. To understand the reducibility of the oxidic catalysts prepared from the different supports, H_2-TPR experiments were conducted and the results are shown in Fig. 12. It can be seen that the H_2-TPR profile of the NiW/Al-SBA-15 catalyst exhibits three main reduction peaks, located at 488, 677, and 852 °C. The reduction peaks located at 488 and 677 °C can be attributed to dispersed polytungstate species with different degrees of reducibility; the highest-temperature peak at 852 °C can be attributed to tetrahedrally coordinated tungsten species, which are hard to reduce, due to interaction with the Al-modified support via Al–O–W linkages [42]. Compared with that of the NiW/Al-SBA-15

Table 3
Amounts of B and L acid sites of the different supports and catalysts determined by pyridine-FTIR.

Sample	Amount of acid sites (μmol g^{-1})					
	200 °C[a]			350 °C[a]		
	L	B	L + B	L	B	L + B
Al-SBA-15	209.4	42.8	272.2	186.0	32.0	218.0
NiW/Al-SBA-15	331.5	23.8	355.3	238.8	19.8	258.6
SBA-15[b]	31.1	–	31.1	35.9	–	35.9
NiW/SBA-15	75.2	–	75.2	46.6	–	46.6
γ-Al_2O_3[b]	212.6	–	212.6	178.2	–	178.2
NiW/γ-Al_2O_3	378.5	13.7	392.2	290.1	–	290.1

[a] Degassing temperature.
[b] Pyridine-FTIR spectra of SBA-15 and γ-Al_2O_3 are not shown in this paper.

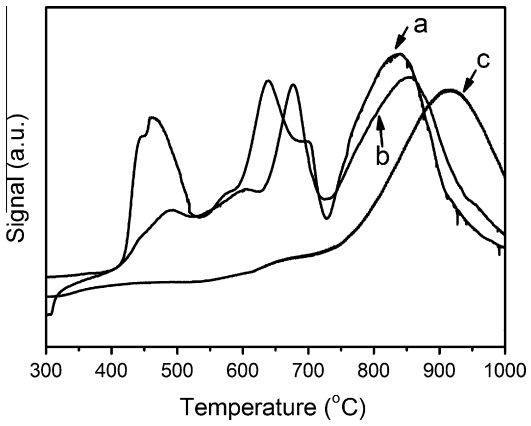

Fig. 12. H_2-TPR profiles of the NiW/SBA-15 (a), NiW/Al-SBA-15 (b), and NiW/γ-Al_2O_3 (c) catalysts.

catalyst, the H_2-TPR profile of the NiW/SBA-15 catalyst shows three peaks at 458, 638 and 836 °C, notably shifting to lower temperatures and thus indicating the weaker metal–support interaction due to the less reactive surface hydroxyl groups attached to Si present in the SBA-15 support. The H_2-TPR profile of the NiW/γ-Al_2O_3 catalyst shows only a single reduction peak at 916 °C, assigned to the reduction of tetrahedrally coordinated tungsten oxide species or the low-condensed oligomeric tungsten oxide species on alumina, which are mostly stabilized on the alumina-containing support [24]. In summary, the above results show that the strength of metal–support interaction for the three catalysts increases in the order NiW/SBA-15 < NiW/Al-SBA-15 < NiW/γ-Al_2O_3. This is because the incorporation of Al atoms into SBA-15 support creates a large number of more reactive Al–OH groups that interact with W species to generate Al–O–W bonds, which have stronger interaction than Si–O–W bonds [7], leading to the appearance of highly dispersed octahedral and tetrahedral W^{6+} species (in line with the disappearance of WO_3 peaks in Fig. 9B). So the NiW/Al-SBA-15 catalyst has better dispersion of active metal oxides than NiW/SBA-15 and therefore more active sites, inducing higher catalytic activity [40]. It is also noted that compared with the NiW/γ-Al_2O_3 catalyst, the NiW/Al-SBA-15 catalyst has much weaker metal–support interaction, so the resulting tungsten species can easily be reduced and sulfided.

To obtain information on the dispersion of the sulfided metal species, HRTEM studies were carried out and the results are shown in Fig. 13. In the NiW/SBA-15 catalyst (Fig. 13A), a large number of WS_2 particles, long and curved (in some cases entangled), are observed on the external surface, causing the blockage of pore mouths. The highly stacked WS_2 slabs on the NiW/SBA-15 catalyst are attributed to the weaker metal–support interaction [10]. The NiW/Al-SBA-15 catalyst (Fig. 13B) presents a lower stacking degree but a higher dispersion of WS_2 slabs than the NiW/SBA-15 catalyst. In the reference catalyst NiW/γ-Al_2O_3 (Fig. 13C), WS_2 particles stacked with only one or two slabs are observed, which is a consequence of the strong interaction of the alumina support with W species [43]. To make a quantitative comparison, the lengths and layer numbers of WS_2 slabs on the sulfided catalysts were obtained through statistical analyses based on 20 micrographs including about 300 slabs obtained from different parts of each catalyst. It can be observed that the morphology of WS_2 crystallites on the different catalysts, namely, the length and stacking layer number, changes depending on the supports of the corresponding catalysts. The average slab length (L_{av}) and stacking layer number (N_{av}) were calculated according to the first moment of the distribution [44], expressed by

$$L_{av}(N_{av}) = \frac{\sum_{i=1}^{n} x_i M_i}{\sum_{i=1}^{n} x_i}, \quad (5)$$

where M_i is the slab length or stacking layer number of a stacked WS_2 unit, and x_i is the number of slabs or stacks in a given range of length or stacking layer number. Table 4 gives the slab length distributions and stacking layer number distributions of the three catalysts. It can be seen that the average length and stacking layer number of WS_2 slabs in NiW/Al-SBA-15 are 4.8 nm and 2.2, respectively, which stand between those (7.4 nm and 2.9 and 4.9 nm and 1.7) in NiW/SBA-15 and NiW/γ-Al_2O_3, signifying that a compromise between dispersion and stacking has been achieved.

Numerous researches have shown that there exist so called "Co(Ni)–Mo(W)–S" phases in which S vacancies occurring at brim/edge sites of MoS_2 crystallites are considered to be active sites for HDS reactions [45]. Depending on the nature of metal–support interactions, the Co(Ni)–Mo(W)–S structure may be present as either type I or type II, which have different catalytic properties. The type I phase is less stacked and thus not fully sulfided, containing some Mo(W)–O–Al linkages with the alumina support related to the strong interaction between Mo(W) and hydroxyl groups on the alumina surface and thus having lower activity. On the other hand, if the interaction between Mo(W) and hydroxyl groups on the alumina surface is dramatically decreased, the resulting structures have increased intrinsic activity. This kind of structure is termed the type II Co–Mo–S phase. A highly stacked type II metal sulfide phase can favor the adsorption and HDS of DBT and its derivatives through the prehydrogenation pathway, because the HDS of DBT and its derivatives with larger molecular size is a geometry-demanding reaction [46]. The NiW/SBA-15 catalyst has the highest degree of stacking, and this should reduce the number of brim sites that are necessary for sulfur elimination via the perpendicular adsorption of the molecule through the S atom [33,45,46]; the NiW/γ-Al_2O_3 catalyst has the lowest degree of

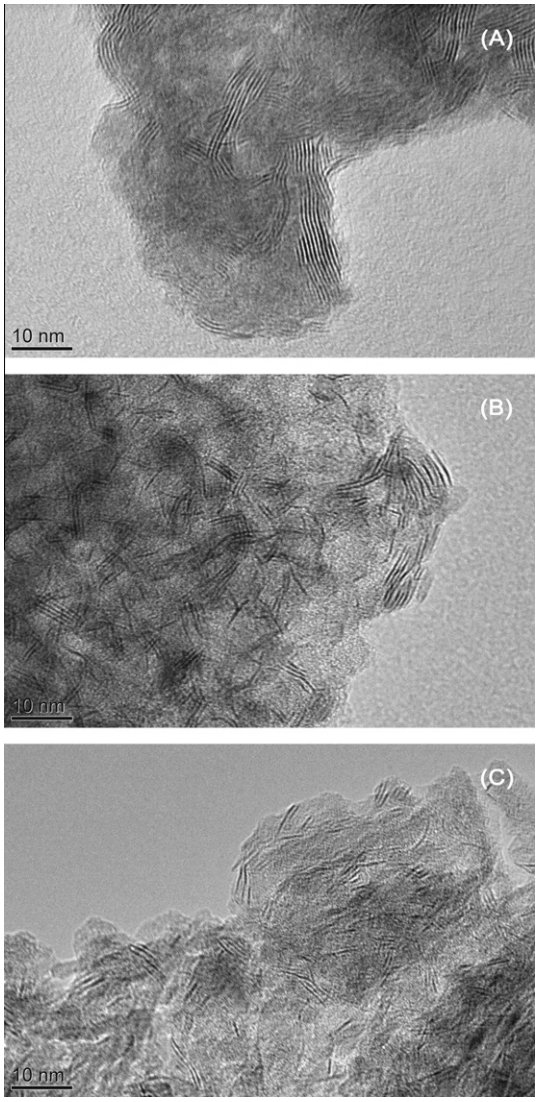

Fig. 13. HRTEM images of the sulfided catalysts NiW/SBA-15 (A), NiW/Al-SBA-15 (B), and NiW/γ-Al_2O_3 (C).

Table 4
Average length (L_{av}) and average stacking layers (N_{av}) of WS_2 crystallites.

Catalyst	NiW/SBA-15	NiW/Al-SBA-15	NiW/γ-Al_2O_3
L_{av} (nm)	7.4	4.8	4.9
N_{av}	2.9	2.2	1.7

stacking, with most active sites being of type I, which is unfavorable for the planar adsorption of the DBT molecule through the aromatic rings and decreases the intrinsic hydrogenation ability [24]; the NiW/Al-SBA-15 catalyst has compromised dispersion and stacking of WS_2 slabs, creating more type II active sites with more brim active sites than the other two catalysts while having a moderate dispersion of WS_2 slabs.

The foregoing results indicate that even after the impregnation of W and Ni, the NiW/Al-SBA-15 catalyst still preserves the characteristic hexagonal structure of SBA-15. Compared with the NiW/SBA-15 and previously reported NiW/Al-SBA-15 catalysts [9,10,33], the NiW/Al-SBA-15 catalyst prepared by us has three advantages: (1) the better dispersion of W and Ni on the surface, as determined by the wide-angle XRD characterization results shown in Fig. 9B; (2) the moderate metal–support interaction, which benefits the creation of accessible active sites without sacrificing the number of active sites; and (3) the larger numbers of B and L acid sites, which would favor the hydrogenolysis/isomerization and hydrogenation ability of the catalyst [12,41].

3.3. Catalytic activity

The catalytic activity of the three sulfided NiW catalysts was examined, using DBT HDS as a model reaction, and the product distributions obtained at 360 °C are shown in Table 5. The typical GC chromatograph of HDS products of reactant DBT over the NiW/Al-SBA-15 catalyst is also obtained (see Fig. S2 in Supplementary Information). Generally, there are two reaction pathways for DBT HDS [28]. The first is direct desulfurization (DDS) leading to the formation of BP, and the second is the hydrogenation route (HYD), consisting of the prehydrogenation of one of the aromatic rings of DBT followed by the elimination of the sulfur atom, first yielding tetrahydrodibenzothiophene (THDBT), then the corresponding hexahydrodibenzothiophene (HHDBT), and finally CHB as the principal desulfurized product of HHDBT and THDBT. All

Table 5
Selectivity of the final products over the different catalysts for DBT HDS at 360 °C.

Selectivity (%)[a]	NiW/Al-SBA-15	NiW/SBA-15	NiW/γ-Al_2O_3
BP	71.5	71.7	60.5
CHB	16.6	23.8	30.8
DCH	1.3	1.5	2.4
THDBT	0.5	2.0	2.3
HHDBT	0.5	–	0.7
CHEB	2.9	1.0	1.7
CPMB	4.3	–	1.6
CPCH	1.8	–	–
CPMCH	0.6	–	–

[a] The selectivity data were calculated from the GC–MS analysis results. This method is just a semiquantitative method since, the GC response factors of all the products cannot be obtained.

of these products were observed over the NiW/SBA-15 catalyst, as reported [47]. Moreover, for the NiW/γ-Al_2O_3 catalyst, cyclohexenylbenzene (CHEB) was detected in the final products, as Wang and Prins [48] reported. Under the reaction conditions we used, CHB and CHEB can suffer further hydrogenation and isomerization, yielding dicyclohexyl (DCH) and CPMB, respectively. Additionally, for the NiW/Al-SBA-15 catalyst with higher medium/strong B acidity than the NiW/γ-Al_2O_3 catalyst, further isomerization products from DCH, such as CPCH and CPMCH, were also detected. By combining the results reported in the previous studies [49] and those in the present study, a reaction network for the DBT HDS was depicted in Fig. 14. Reactions 1–6 are typical processes in the DBT HDS reaction over the NiW/SBA-15 catalyst; reactions 7–9 happen over the NiW/γ-Al_2O_3 catalyst with the additional new product CPMB, i.e., the isomerization product of CHEB; reactions 11 and 12 only happen over the acidic catalyst NiW/Al-SBA-15 with the observation of CPCH and CPMCH, i.e., the further isomerization products of DCH. When the acidic Al-SBA-15 is used as the support, the resulting NiW/Al-SBA-15 catalyst has a larger number of L acid

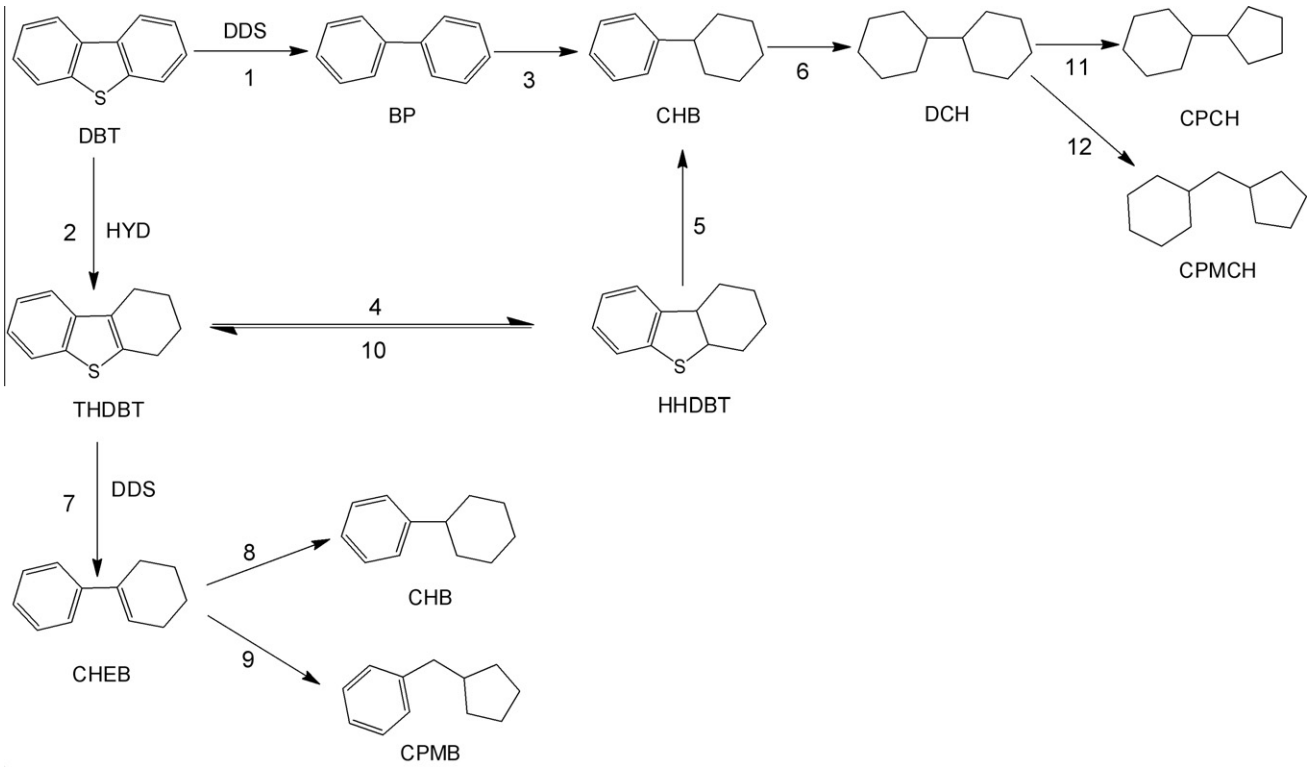

Fig. 14. Reaction network of DBT HDS over the NiW/Al-SBA-15 catalyst.

Table 6
Rate constants (k_{HDS}), TOFs, and HYD/DDS pathway ratios obtained over the different catalysts for DBT HDS at 360 °C.

Catalyst	k_{HDS} (10^{-3} mol g^{-1} h^{-1})	TOF (10^4 s^{-1})	HYD/DDS ratio
NiW/Al-SBA-15	7.51	1.26	0.23
NiW/SBA-15	1.96	0.53	0.33
NiW/γ-Al_2O_3	4.59	1.14	0.51

sites and most importantly the largest number of B acid sites among the three catalysts, as shown in Table 3. These acid sites enhance both the DDS and HYD abilities of the NiW/Al-SBA-15 catalyst. B acid sites especially enhance the hydrogenolysis and isomerization activities of the catalyst, as demonstrated by the existence of the largest amounts of BP and some other further isomerization products. Finally, we must point out that no lighter cracking products (C_3–C_6) of DBT HDS were detected, significantly different from the results reported in previous studies [7,31]. We attribute this to the smaller number of strong B acid sites and thereby negligible cracking ability of the NiW/Al-SBA-15 catalyst.

To distinguish the individual contributions of the DDS and HYD routes to the overall HDS performance of the three catalysts, the ratio of the HYD selectivity to the DDS selectivity is defined as the ratio of the selectivity of CHB to that of BP at the same DBT HDS conversion (50%). The selectivity to the various products is given in Table 5, and the HDS rate constants, TOFs, and HYD/DDS ratios are given in Table 6. Compared with the NiW/SBA-15 and NiW/γ-Al_2O_3 catalysts, the NiW/Al-SBA-15 catalyst exhibits the highest HDS rate constant k_{HDS} and TOF, revealing the best DBT HDS activity among the three catalysts. For all three catalysts studied, the preferential HDS route is the DDS pathway, and the DDS activity for the different catalysts is in the order NiW/γ-Al_2O_3 < NiW/SBA-15 < NiW/Al-SBA-15. These results suggest that the use of Al-SBA-15 as support leads to an improvement in the DDS ability of the catalyst, enhancing the DDS route and thus resulting in an increased HDS rate. This effect could be related to the enhanced B acid sites and the changes in the morphology of the WS_2 active phase induced by the stronger interaction of the oxidic precursor phases with the Al atoms of the support [50,51].

Large pores can eliminate diffusion resistance and enhance accessibility of the active sites to reactant molecules. Many efforts have been made to achieve a suitable pore structure to eliminate steric hindrance in the HDS of DBT or 4,6-DMDBT. Sampieri et al. [52] reported that multilayer MoS_2 slabs loaded inside the MCM-41 pores could lead to serious limitations for DBT to access the active sites, while this did not occur in SBA-15 because of its larger pore size, which suggests that the HDS of DBT over the NiW/Al-SBA-15 catalyst would be in the kinetic-controlled region but not in the diffusion-controlled zone. The DBT HDS performance of the NiW/Al-SBA-15 catalyst was assessed at four different temperatures, 320, 340, 360, and 380 °C, and results are shown in Fig. 15. From Fig. 15A, we can see that the HDS conversion of DBT increases with increasing temperature. Fig. 15B shows that increasing reaction temperature increases the HDS rate via the DDS route but decreases that via the HYD route followed by the DDS route, as reflected by the increasing selectivity to BP and the decreasing selectivity to CHB, respectively. This indicates that to some extent there is a thermodynamic limit for the HYD route. The HDS of sulfur-containing compounds via ring hydrogenation prior to sulfur removal was found to be thermodynamically limited, especially at higher temperatures [53,54], because of the inverse relationship of the adsorption rate and the reaction temperature. Thermodynamically, the hydrogenation of DBT to form THDBT is only favored at temperatures lower than 330 °C, becoming almost negligible at temperatures higher than 425 °C [53]. From Fig. 15B, we can see that the selectivity to other HYD products follows the same trend

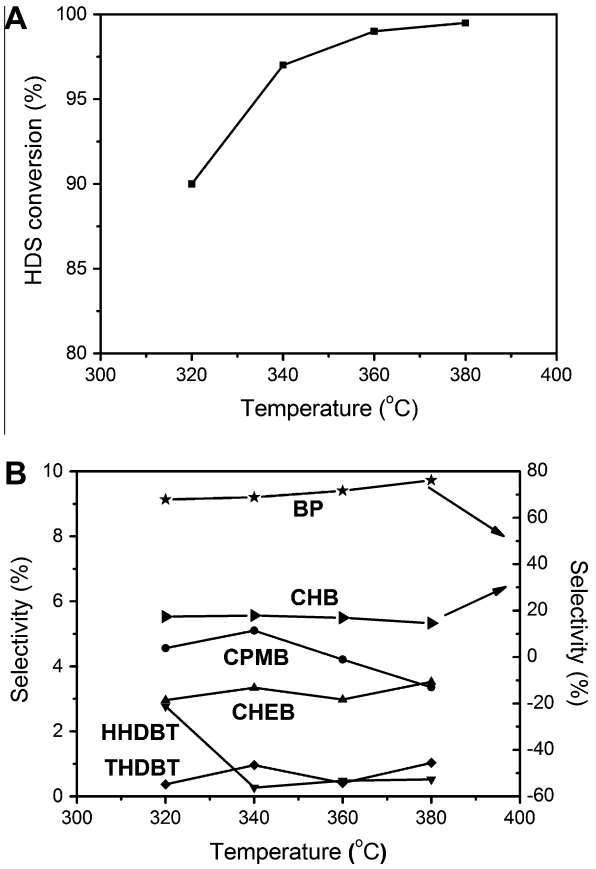

Fig. 15. HDS conversion (A) and selectivity of the final products (B) over NiW/Al-SBA-15 catalyst for DBT HDS at different temperatures.

as reported in previous studies [49,53,54] with the increasing reaction temperature.

To determine whether the incorporation of aluminum can improve the HDS reaction stability of the resulting catalyst NiW/Al-SBA-15, 2 mL of the NiW/Al-SBA-15 catalyst was evaluated, using a FCC diesel as feedstock, for 200 h. As shown by the variation trend of HDS conversion as a function of time on stream in Fig. 16, the NiW/Al-SBA-15 catalyst demonstrated stable HDS activity during the test, giving a desulfurization ratio of 99.5–99.8% and a product sulfur content of lower than 10 ppm.

In summary, the superior DBT HDS performance of the NiW/Al-SBA-15 catalyst could be attributed to the following three factors:

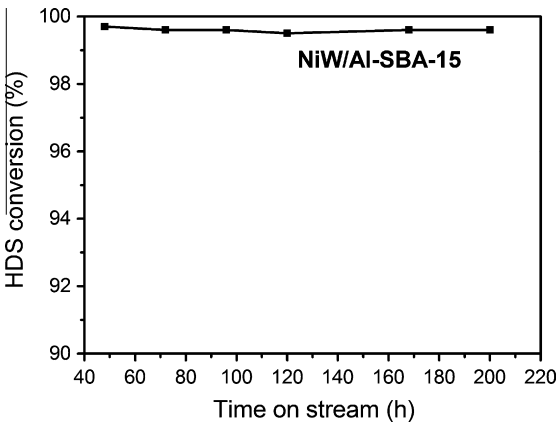

Fig. 16. HDS conversion with time on stream over catalyst NiW/Al-SBA-15.

(1) The better dispersion of the active metals, which is necessary for the creation of a larger number of accessible active sites. The dispersion of oxidic W and Ni species increases with the incorporation of aluminum into the SBA-15 support, as shown by the wide-range XRD characterization results in Fig. 9B. In addition, the homogenous distribution of WS_2 crystals (Fig. 13B) was obtained due to the strong interaction of oxidic W and Ni species with Al–OH on the support, as confirmed by the H_2-TPR characterization results in Fig. 12.

(2) The short length and increased stacking layers of WS_2 slabs, which favor the formation of more type II active phase. In the NiW/Al-SBA-15 catalyst, Ni–W–S phases consist mostly of short slabs (~5 nm) of two layers, as shown by the HRTEM images in Fig. 13B. On one hand, for a large sulfur-containing molecule such as DBT, a lower degree of stacking of sulfide slabs, as in the case of the NiW/γ-Al_2O_3 catalyst, hampers the planar adsorption of the molecule through its aromatic rings and thereby decreases the HDS activity [48]; on the other hand, a very high degree of stacking sulfide slabs, as observed for the weakly interacting support SBA-15, reduces the number of corner sites, which are necessary for sulfur elimination via the perpendicular adsorption of the molecule through the S atom [45].

(3) The more and stronger B acid sites and enhanced L acid sites, which favor the hydrogenolysis/isomerization and hydrogenation ability of the catalyst and enhance the HDS activity. Solis et al. [55] considered that the enhanced DBT HDS activity of metal sulfides over acidic supports is partly related to the improvement in their hydrogenation property due to electronic effects of the acidity on the metal sulfide phase; Gallezot et al. [56] reported that both B and L acid sites can be used as the potential electron acceptors and the resulting electron-deficient metal clusters can promote the π adsorption of DBT via its aromatic rings which is the prerequisite for the HYD pathway. The NiW/Al-SBA-15 catalyst has the highest amount of B acid sites that are expected to enhance the hydrogenolysis and isomerization ability of the catalyst, and truly the DBT HDS products contain the highest amount of DDS pathway product BP and the further isomerization products CPMB, CPCH, and CPMCH, as shown in Table 5. It is the perfect combination of the good dispersion and suitable stacking of metal sulfide crystals and the enhanced B and L acid sites that endows the NiW/Al-SBA-15 catalyst with the best DBT HDS activity.

4. Conclusions

In conclusion, highly ordered and highly hydrothermally stable Al-SBA-15 materials have been prepared by adjusting pH and increasing temperature during the hydrothermal treatment process. Using such a method, almost all Al species have been successfully introduced into SBA-15. Thus-obtained Al-SBA-15 has uniformly distributed mesopores, high hydrothermal stability, and medium B/L acidity. Using Al-SBA-15 as support, a NiW/Al-SBA-15 catalyst was prepared and showed much higher DBT HDS activity than SBA-15 and Al_2O_3 supported catalysts because of the perfect combination of the better dispersion and higher stacking of Ni–W–S phases on the support and the participation of B and L acid sites. This study opens a new route to the introduction of Al and other heteroatoms into mesoporous silica materials with various mesostructures and demonstrates the potential of mesostructured silicoaluminate Al-SBA-15 with high aluminum loading and suitable B and L acidity as support for deep HDS catalysts.

Acknowledgments

This work was financially supported by the National Basic Research Program of China (the 973 Program) (Grant 2010CB226901), the National Natural Science Foundation of China (Grants 20573021 and 20825621), the Ministry of Education of China (Grant 20060246010), and the Society of Technical Communication (Shanghai) (Grant 08DZ2270500).

Appendix A. Supplementary material

Supplementary data associated with this article can be found, in the online version, at doi:10.1016/j.jcat.2011.10.023.

References

[1] D.Y. Zhao, J.L. Feng, Q.S. Huo, N. Melosh, G.H. Fredrickson, B.F. Chmelka, G.D. Stucky, Science 279 (1998) 548.
[2] D.Y. Zhao, Q.S. Huo, J.L. Feng, B.F. Chmelka, G.D. Stucky, J. Am. Chem. Soc. 120 (1998) 6024.
[3] J.S. Beck, J.C. Vartuli, W.J. Roth, M.E. Leonowicz, C.T. Kresge, K.D. Schmitt, T.W. Chu, D.H. Olson, E.W. Sheppard, S.B. McCullen, J.B. Higgins, J.L. Schlenkert, J. Am. Chem. Soc. 114 (1999) 10834.
[4] C.T. Kresge, M.E. Leonowicz, W.J. Roth, J.C. Vartuli, J.S. Beck, Nature 359 (1992) 710.
[5] A. Corma, Chem. Rev. 97 (1997) 2373.
[6] Q.F. Tan, Y. Fan, H.Y. Liu, T.C. Song, G. Shi, B.J. Shen, X.J. Bao, AIChE J. 54 (2008) 1850.
[7] L.Y. Lizama, T.E. Klimova, J. Mater. Sci. 44 (2009) 6617.
[8] G.M. Kumaran, S. Garg, K. Soni, M. Kumar, L.D. Sharma, G.M. Dhar, K.S.R. Rao, Appl. Catal. A Gen. 305 (2006) 123.
[9] A. Olivas, T.A. Zepeda, Catal. Today 143 (2009) 120.
[10] G.M. Esquivel, J. Ramírez, A. Gutiérrez-Alejandre, Catal. Today 148 (2009) 36.
[11] X. Li, A.J. Wang, M. Egorova, R. Prins, J. Catal. 250 (2007) 283.
[12] Y.Y. Sun, R. Prins, Angew. Chem. Int. Ed. 47 (2008) 8478.
[13] F. Hoffmann, M. Cornelius, J. Morell, M. Fröba, Angew. Chem. Int. Ed. 45 (2006) 3216.
[14] B. Dragoi, E. Dumitriu, C. Guimon, A. Auroux, Micropor. Mesopor. Mater. 121 (2009) 7.
[15] H.M. Kao, C.C. Ting, S.W. Chao, J. Mol. Catal. A Chem. 235 (2005) 200.
[16] S. Sumiya, Y. Oumi, T. Uozumi, T. Sano, J. Mater. Chem. 11 (2001) 1111.
[17] Z.H. Luan, E.M. Maes, P.A.W. Van der Heide, D.Y. Zhao, R.S. Czernuszewicz, L. Kevan, Chem. Mater. 11 (1999) 3680.
[18] A. Campos, L. Martins, L. Deoliveira, C. Dasilva, M. Wallau, E. Urquietagonzalez, Catal. Today 107–108 (2005) 759.
[19] R. Mokaya, J. Phys. Chem. B 104 (2000) 8279.
[20] Y.D. Xia, R. Mokaya, Micropor. Mesopor. Mater. 74 (2004) 179.
[21] D.H. Pan, P. Yuan, L.Z. Zhao, N. Liu, L. Zhou, G.F. Wei, J. Zhang, Y.C. Ling, Y. Fan, B.Y. Wei, H. Liu, C.Z. Yu, X.J. Bao, Chem. Mater. 21 (2009) 5413.
[22] L.L. Hench, J.K. West, Chem. Rev. 90 (1990) 33.
[23] X.Y. Lin, Y. Fan, Z.H. Liu, G. Shi, H.Y. Liu, X.J. Bao, Catal. Today 125 (2007) 185.
[24] H. Wang, Y. Fan, G. Shi, H.Y. Liu, X.J. Bao, J. Catal. 260 (2008) 119.
[25] H.S. Joo, J.A. Guin, Fuel Process. Technol. 49 (1996) 137.
[26] S. Brunauer, P.H. Emmett, E. Teller, J. Am. Chem. Soc. 60 (1938) 309.
[27] E.P. Barrett, L.G. Joyner, P.P. Halenda, J. Am. Chem. Soc. 73 (1951) 373.
[28] G. Berhault, M.P. De Ia Rosa, A. Mehta, M.J. Yácaman, R.R. Chianelli, Appl. Catal. A Gen. 345 (2008) 80.
[29] E.J.M. Hensen, P.J. Kooyman, Y. van der Meer, A.M. van der Kraan, V.H.J. de Beer, J.A.R. van Veen, R.A. van Santen, J. Catal. 199 (2001) 224.
[30] Y. Liu, W.Z. Zhang, T.J. Pinnavaia, Angew. Chem. Int. Ed. 40 (2001) 1255.
[31] S.Q. Zeng, J. Blanchard, M. Breysse, Y.H. Shi, X.T. Su, H. Nie, D.D. Li, Appl. Catal. A Gen. 298 (2006) 88.
[32] S.Q. Zeng, J. Blanchard, M. Breysse, Y.H. Shi, X.T. Su, H. Nie, D.D. Li, Micropor. Mesopor. Mater. 85 (2005) 297.
[33] A. Sampieri, S. Pronier, S. Brunet, X. Carrier, C. Louis, J. Blanchard, K. Fajerwerg, M. Breysse, Micropor. Mesopor. Mater. 130 (2010) 130.
[34] X.D. Li, M.J. Edirisinghe, Chem. Mater. 16 (2004) 1111.
[35] T. Kataoka, J.A. Dumesic, J. Catal. 112 (1988) 66.
[36] P. Rayo, J. Ramírez, M.S. Rana, J. Ancheyta, A. Aguilar-Elguézabal, Ind. Eng. Chem. Res. 48 (2009) 1242.
[37] V. Sundaramurthy, I. Eswaramoorthi, A.K. Dalai, J. Adjaye, Micropor. Mesopor. Mater. 111 (2008) 560.
[38] D. Li, A. Nishijima, D.E. Morris, G.D. Guthrie, J. Catal. 188 (1999) 111.
[39] T. Klimova, J. Reyes, O. Gutiérrez, L. Lizama, Appl. Catal. A Gen. 335 (2008) 159.
[40] L. Vradman, M.V. Landau, M. Herskowitz, V. Ezersky, M. Talianker, S. Nikitenko, Y. Koltypin, A. Gedanken, J. Catal. 213 (2003) 163.
[41] M.Y. Sun, D. Nicosia, R. Prins, Catal. Today 86 (2003) 173.
[42] D.C. Vermaire, P.C.V. Berge, J. Catal. 116 (1989) 309.
[43] H. Topsøe, B.S. Clausen, F.E. Massoth, Hydrotreating Catalysis—Science and Technology, Springer, Berlin, 1996.

[44] Y. Fan, H. Xiao, G. Shi, H.Y. Liu, Y. Qian, T.H. Wang, G.B. Gong, X.J. Bao, J. Catal. 279 (2011) 27.
[45] H. Topsøe, Appl. Catal. A Gen. 322 (2007) 3.
[46] C.S. Song, Catal. Today 86 (2003) 211.
[47] T. Klimova, L. Peña, L. Lizama, C. Salcedo, O.Y. Gutiérrez, Ind. Eng. Chem. Res. 48 (2009) 1126.
[48] H.M. Wang, R. Prins, J. Catal. 258 (2008) 153.
[49] C.M. Wang, T.C. Tsai, I. Wang, J. Catal. 262 (2009) 206.
[50] T. Klimova, M. Calderón, J. Ramírez, Appl. Catal. A Gen. 240 (2003) 29.
[51] O.Y. Gutiérrez, T. Klimova, J. Catal. 281 (2011) 50.
[52] A. Sampieri, S. Pronier, J. Blanchard, M. Breysse, S. Brunet, K. Fajerwerg, C. Louis, G. Pérot, Catal. Today 107–108 (2005) 537.
[53] D.D. Whitehurst, T. Isoda, I. Mochida, Adv. Catal. 42 (1998) 345.
[54] H. Farag, D.D. Whitehurst, K. Sakanishi, I. Mochida, Catal. Today 50 (1999) 49.
[55] D. Solis, A. Agudo, J. Ramirez, T. Klimova, Catal. Today 116 (2006) 469.
[56] P. Gallezot, S. Chaumet, A. Perrard, P. Isnard, J. Catal. 168 (1997) 104.